Journal of Achievements in Materials and Manufacturing Engineering
VOLUME 40
ISSUE 1
May
2010

Application of off-line error correction method software to reproduce random signals on servo-hydraulic testers

D. Braska [a,*], P. Czop [a], D. Sławik [a], G. Wszołek [b]
[a] Tenneco Automotive Eastern Europe, Eastern European Engineering Center (EEEC), Control and Measuring Systems Department, ul. Bojkowska 59 B, 44-100 Gliwice, Poland,
[b] Institute of Engineering Processes Automation and Integrated Manufacturing Systems, Silesian University of Technology, ul. Konarskiego 18a, 44-100 Gliwice, Poland
* Corresponding author: E-mail address: damian.braska@tenneco.com

Received 03.03.2010; published in revised form 01.05.2010

Analysis and modelling

ABSTRACT

Purpose: This paper presents an approach towards improving the test rig performance for road signals used in automotive shock absorber tests. The goal is to develop a method for correction of the test signal profile in the off-line mode. The method is intended to be implemented as a software solution without any changes either in hardware or the settings of the servo-hydraulic tester.
Design/methodology/approach: A two-stage validation of the proposed correction method was conducted using a servo-hydraulic test rig and its first-principles model. The model is capable of capturing key dynamical properties over a wide operating range while being only moderately complex. Both simulation and experimental performance results are presented and discussed.
Findings: The proposed method, both in the frequency and time domain, improves the tracking of the test signal by 10-20% and allows an accuracy of more than 90% to be gained using the best fit measure in the case of reproduction of white noise signals.
Research limitations/implications: It is possible to consider more advanced model-based methods for performing off-line error correction. These methods can be used if an accuracy close to 100% is expected.
Practical implications: The result of the investigations is the algorithm implemented in the LabView software to automatically perform the correction of the test signal before the test.
Originality/value: The paper proposes a modern approach towards the validation process by applying a simulation environment. This ensures the involvement of arbitrary disturbance models to investigate key parameters of the correction method without expensive and time-consuming experimental validation. The developed model can be extended to a model of a shock absorber to simulate full interaction between the servo-hydraulic test rig and the tested product.
Keywords: Off-line error cancellation; Signal profile correction; Hydraulic actuator performance

Reference to this paper should be given in the following way:
D. Braska, P. Czop, D. Sławik, G. Wszołek, Application of off-line error correction method software to reproduce random signals on servo-hydraulic testers, Journal of Achievements in Materials and Manufacturing Engineering 40/1 (2010) 41-49.

1. Introduction

A crucial stage of shock absorber manufacturing is the validation process [1-2]. Shock absorbers are evaluated regarding comfort, noise and lifetime, using synthesized or road load data [3-4]. A segment load signal, repeating in-the-loop has to be accurately tracked by test rigs, which the most frequently are found application in the validation process of shock absorbers. While performing either durability or comfort evaluation tests, obtaining repeatable and reproducible results is one of the most important steps in automotive shock absorber development [5]. In this case, the challenge is to apply the realization of the loading sequence to a shock absorber, minimizing the error between the reference and measured signals. Moreover, it is important in the automotive industry to standardize tests which are typically performed in a few locations using servo-hydraulic tests rigs from different manufacturers. The test results are affected by numerous contributors, such as calibration accuracy, properties of the actuator and oil, ambient and oil temperature, and finally by different control strategies applied for particular test rigs. In such a case, designing a robust control process and obtaining the same accuracy in reproducing test signals is extremely unlikely and might be problematic using conventional on-line control algorithms.

In the literature, several papers [6] discuss off-line feedback or feed-forward controllers to tackle this problem. The controllers perform an iterative off-line correction process with the use of an inverse model of the test rig [7]. The model is identified using system identification techniques. However, this paper proposes a basic iterative method of off-line error correction which in each iteration obtains the difference between the reference (command) and measured (test rig response) signals. The error decreases gradually in a few iterations, achieving excellent tracking of random signals on a servo-hydraulic tester. When iterations are performed on the test rig, the standard PID-FF controller is set to the optimal setting that minimizes the error in the on-line mode. The methods were validated with the use of the servo-hydraulic test rig [8] and its model using two types of random signals, i.e. white and pink noise. The model allowed numerical tests to be performed without the influence of disturbances which are normally present during experimental tests, e.g. oil supply system. The paper presents the architecture of the servo-hydraulic test rig and briefly describes each component of its model. The significance of each physical parameter, as well as the degree to which each parameter influences the behaviour of the model, is discussed in Section 2. The problem of modelling control systems is also addressed in the paper. The simulations described in this paper were aimed primarily at obtaining a qualitative insight into the modelled vibration phenomena, and allowed the irrelevant effects to be disregarded in later stages of the model development process

The remaining content of the paper is divided into 5 sections. Section 2 discusses a servo-hydraulic test rig and its model, while Section 3 describes the evaluation criteria for the proposed approach. Sections 4 illustrates and discusses the experimental and simulation results and Section 5 includes final thoughts and a summary of what is presented in the paper.

2. Servo-hydraulic test rig

Experimental tests were performed on a Hydropuls® MSP25 servo-hydraulic test-rig, equipped with an IST8000 electronic controller (Fig. 1). The test rig was used to load a shock absorber and capture its dynamic characteristics, i.e. displacement vs. force. Data acquisition was performed with an 8-channel ICP amplifier manufactured by LMS. The test rig is equipped with an oil supply system (the so-called servo-pack) that provides a pressure of 28 MPa at a flow-rate of 90 l/min. The actuator provides a 25 kN force at the rod, while the maximum stroke is 250 mm at the maximum achievable velocity of 3 m/s. The actuator rod is coupled to the adapter, which transfers the force to a shock absorber mounted on a test rig.

Fig. 1. A servo-hydraulic test-rig used in experimental investigations

The main components of the servo-hydraulic system are the hydraulic actuator with integrated displacement transducer in a piston-rod assembly (IST-Schenk) and the three-stage servo-valve system. The test rig is equipped with a PID-FF controller. The feed-forward (FF) section in this controller passes a proportion of the command signal to the controller output through a high-pass filter to block the command mean level. Different control settings are used depending on the type of excitation signal. The excitation signal is converted into a voltage applied to the servo-valve, which controls the amount of oil supplied to the chambers of the actuator.

The Hydropuls® MSP25 model consists of a servo-valve and a hydraulic actuator model. The Moog G761 series (Fig. 2) industrial servo-valve consists of a polarized electrical torque motor and two stages of hydraulic power amplification. This valve is modelled by a transfer function whose input is a voltage and output is the spool displacement [9].

The electromagnetic torque motor, driving the flapper, is controlled by an electrical current inputted from a current amplifier. A valve control input u (voltage) is converted into a current, with a current amplifier gain Ke. The hydrodynamic

forces acting on the spool are neglected. Therefore, the spool position only depends on the input voltage

$$G_{servo} = \frac{x_{spool}(s)}{u(s)} = \frac{K_e \cdot K_{spool}}{1 + \left(\frac{2\zeta}{\omega_{n,servo}}\right)s + \left(\frac{s}{\omega_{n,servo}}\right)^2} \quad (1)$$

where

$$\omega_{n,servo} = \sqrt{\frac{k_{servo}}{m_{servo}}}; \quad \zeta = \frac{b_{servo}}{2}\sqrt{\frac{1}{k_{servo} \cdot m_{servo}}} \quad (2)$$

Spool movements are limited by the values of stiffness

$$k_{servo} = \begin{cases} k_{servo,\inf} & if \quad x_{spool} > x_{spool,\max} \\ k_{servo,nom} & if \quad x_{spool,\min} \le x_{spool} \le x_{spool,\max} \\ k_{servo,\inf} & if \quad x_{spool} < x_{spool,\min} \end{cases} \quad (3)$$

The pressure drops among the test rig chambers (A and B), input (P) and output (T) are as follows

$$\begin{aligned} \Delta p_{PA} &= p_P - p_A \\ \Delta p_{BT} &= p_B - p_T \\ \Delta p_{AT} &= p_A - p_T \\ \Delta p_{PB} &= p_P - p_B \end{aligned} \quad (4)$$

The flows at all servovalve restrictions are determined by orifice equations based on pressure drops and spool displacement,

$$\begin{aligned} & q_{PA} = Cd_{PA} \cdot b \cdot |\Delta x_{spool}| \cdot \sqrt{|\Delta p_{PA}|} \cdot \mathrm{sgn}(\Delta p_{PA}) \\ & if \quad \Delta x_{spool} = x_{spool} - x_{spool,0} \ge 0 \\ & q_{BT} = Cd_{BT} \cdot b \cdot |\Delta x_{spool}| \cdot \sqrt{|\Delta p_{BT}|} \cdot \mathrm{sgn}(\Delta p_{BT}) \\ & if \quad \Delta x_{spool} = x_{spool} - x_{spool,0} \ge 0 \\ & q_{AT} = Cd_{AT} \cdot b \cdot |\Delta x_{spool}| \cdot \sqrt{|\Delta p_{AT}|} \cdot \mathrm{sgn}(\Delta p_{AT}) \\ & if \quad \Delta x_{spool} = x_{spool} + x_{spool,0} < 0 \\ & q_{PB} = Cd_{PB} \cdot b \cdot |\Delta x_{spool}| \cdot \sqrt{|\Delta p_{PB}|} \cdot \mathrm{sgn}(\Delta p_{PB}) \\ & if \quad \Delta x_{spool} = x_{spool} + x_{spool,0} < 0 \end{aligned} \quad (5)$$

A model of a hydraulic actuator is derived assuming the pressures in the actuator chambers and displacement of the rod as the state variables [23] (Fig. 11). The bypass flow, controlled by the throttle valve, is defined by the following formula

$$q_{AB} = Cd_{AB} \cdot A_{leakage} \cdot \sqrt{|\Delta p_{AB}|} \cdot \mathrm{sgn}(\Delta p_{AB}) \quad (6)$$

The total balance of the inlet and outlet flows is determined as follows

$$\begin{aligned} q_A &= q_{PA} - q_{AT} - q_{AB} \\ q_B &= q_{PB} - q_{BT} + q_{AB} \end{aligned} \quad (7)$$

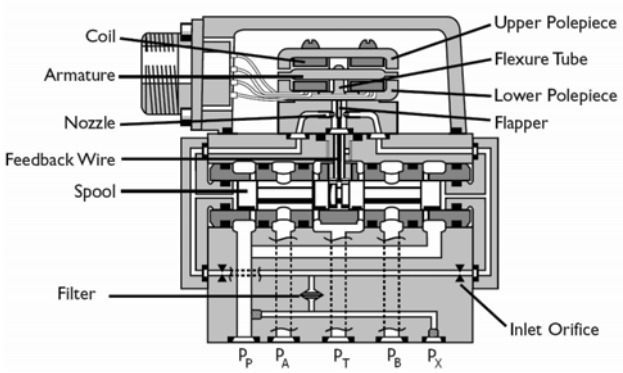

Fig. 2. The MOOG G761 servo-valve assembly [10]

The pressures p_A and p_B are determined based on the mass equilibrium equations, where the volumes are determined based on the initial oil volume in the actuator and the position of the piston-rod

$$\begin{aligned} \frac{dp_A}{dt} &= \frac{(q_A - V_A) \cdot \beta}{V_{A0} + A_A \cdot x_4} \\ \frac{dp_B}{dt} &= \frac{(q_B + V_B) \cdot \beta}{V_{B0} - A_B \cdot x_4} \end{aligned} \quad (8)$$

were changes of chamber volumes

$$\dot{V}_A = A_A \dot{x}_4, \; \dot{V}_B = A_B \dot{x}_4 \quad (9)$$

Finally, the displacement of the actuator x_4 is calculated based on the force equilibrium equation

$$\ddot{x}_4 m_4 + \ddot{x}_4 c_{act} = p_A A_A - p_B A_B - F_4(x, \dot{x}) \quad (10)$$

A model of the electronic controller uses a program command and sensor feedback to control the servovalve. A test rig controller uses a group of gain controls, i.e. proportional (P), integral (I), derivative (D) and feed-forward (FF) gains. A transfer function representation of a PID-FF controller is given as follows

$$\begin{aligned} G_{PID} &= \frac{u_{PID}(s)}{\Delta x_4(s)} = K_P\left(1 + \frac{1}{sT_I} + sT_D\right) = \ldots \\ &= K_P + \frac{K_I}{s} + K_D s \end{aligned} \quad (11)$$

where

$$\Delta x_4 = x_{4,expected} - x_4 \cdot \tag{12}$$

A feed-forward is an open loop correction which can be used to reduce the phase lag between the reference and feedback signals. A transfer function representation of a feed-forward (FF) gain is as follows

$$G_{FF} = \frac{u_{FF}(s)}{x_{4,expected}(s)} = K_F \cdot \frac{sT_f}{1+sT_f}, \tag{13}$$

The time-constant of the feed-forward (FF) filter controls the upper frequency at which the differentiations of the reference signal is effective. A small time constant (i.e. high frequency) passes high-frequency disturbances while an exceeded value does not produce true velocity at the test frequency. The combined output of the PID-FF controller is determined as follow

$$u = u_{PID} + u_{FF}, \tag{14}$$

The equations have been implemented in the MATLAB/Simulink package [13].

3. Evaluation of the proposed methods

Two test signals, namely pink and white noise, were used to validate the proposed method in the time and frequency domain. The screen-shot of the test signals is presented in

Fig. 3 and their properties in Table 1 where amplitude extremes are given.

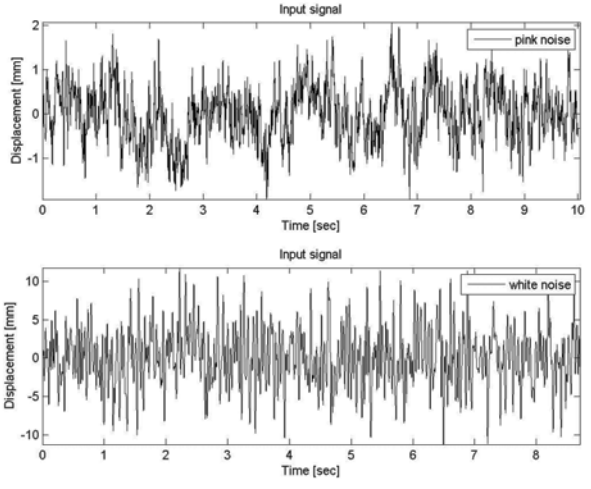

Fig. 3. Test excitation signals

Table 1.
Extremes of the test signals

	Min [mm]	Max [mm]
Pink noise	-1.93	2.05
White noise	-11.33	11.73

Those command signals were tested both on model and test rig in order to compare their responses.

Correction method for new drive signal uses a frequency domain basis algorithm to perform the correction. All the calculations are handled within a program, which requires only demand (command), response and the target (wanted) signal.

The correction is carried out in the frequency domain on a series of overlapping frames. For each frame of the time history acquired, target and demand data are windowed, transformed to the frequency domain and processed. The estimated corrected drive signal is converted back to the time domain, windowed again and the results overlap added to generate the new demand history. Described algorithm flow follows the conventional iterative control equation

$$u_{k+1}(t) = u_k(t) + \alpha(t) \cdot h(t) \cdot e_k(t), \tag{15}$$

Where $u_k(t)$ is the command signal at the k^{th} iteration, $\forall(t)*h(t)$ is the weighted transfer function and $e_k(t) = y_d(t) - y_k(t)$ is the tracking error.

The use of a single frame may be a poor estimate of the transfer function however because the ratio is calculated using the actual demand profile it is a good estimate of the correction required to achieve the desired profile. Because the correction factor is calculated on a frame-by-frame basis there may be positive advantages when the system response changes throughout a test, because of hydraulic flow limitations, for example.

The performance of the correction algorithm can be evaluated either by visual inspection of the plot of the u(i) and $u^*(i)$ or by analyzing the value of

$$R^2 = 1 - \frac{\frac{1}{N}\sum_{i=1}^{N}\left|u(i) - u^*(i)\right|^2}{\frac{1}{N}\sum_{i=1}^{N}\left|u(i)\right|^2}, \tag{16}$$

where u(i) is the reference signal in the time or frequency domain, and $u(i)^*$ is the measured signal in the time or frequency domain respectively. The R is that part of the load variation that is explained by the inverse model and, for convenience, is expressed in %.

4. Simulation and experimental results

Having the commands and responses both from the model and the servo-hydraulic test rig, the initial fit can be obtained. Corresponding results are shown in Table 2.

Table 2.
Initial fit results

	Model fit [%]	Test-rig fit [%]
Pink noise	74.6	72.0
White noise	88.9	91.4

In order to be sure of the results, 3 iterations of one proposed method were performed.

FFT limited up to 50 Hz was used. This is a convenient method since it is the fastest from all validated. It is also actual taking into account hardware limitation of the test rig.

Simultaneously, model and test rig iterates 3 times creating new commands for the system. Results are presented in Table 3 and Table 4.

Table 3.
FFT method validation for pink noise excitation

	Pink noise	
	Model fit [%]	Test rig fit [%]
Original	74.6	72
1 iteration	82.9	82.1
2 iteration	83.5	83.6
3 iteration	83.8	84.1

Table 4.
FFT method validation for white noise excitation

	White noise	
	Model fit [%]	Test rig fit [%]
Original	88.9	91.4
1 iteration	95.2	96.2
2 iteration	95.5	97
3 iteration	95.8	97.3

Graphical results of the correction process for pink noise drive signal are presented at following figures: Fig. 4, Fig. 5, Fig. 6 for test rig model, Fig. 7, Fig. 8, Fig. 9 for physical test rig.
To clearly present following iterations only short time window is chosen.

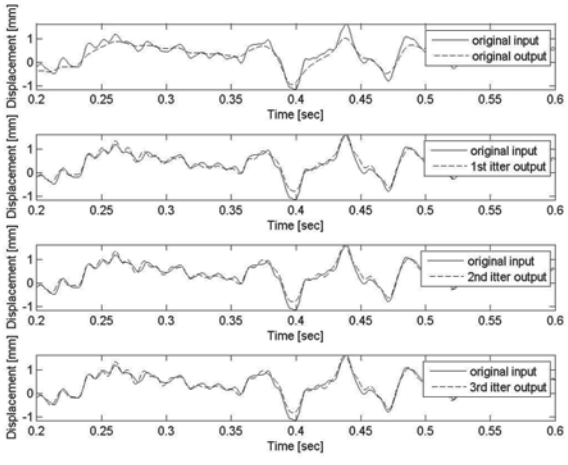

Fig. 4. Pink noise profile correction using test rig model

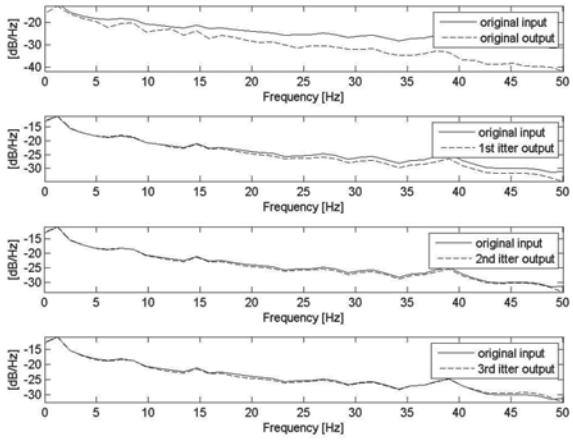

Fig. 5. PSD of pink noise for test rig model (displacement)

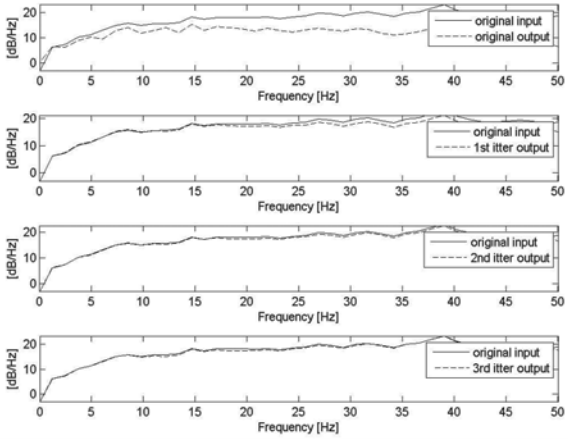

Fig. 6. PSD of pink noise for test rig model (velocity)

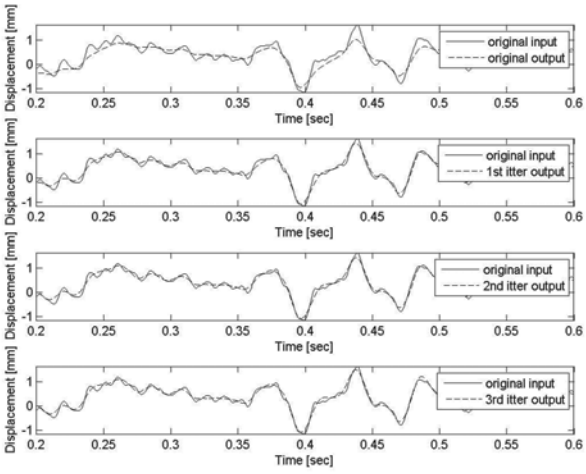

Fig. 7. Pink noise profile correction using test rig

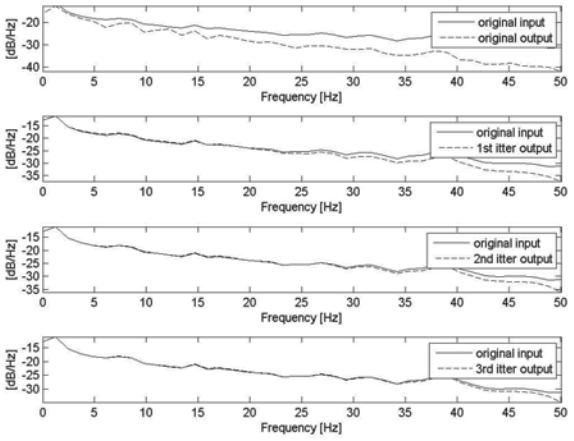

Fig. 8. PSD of pink noise for test rig (displacement)

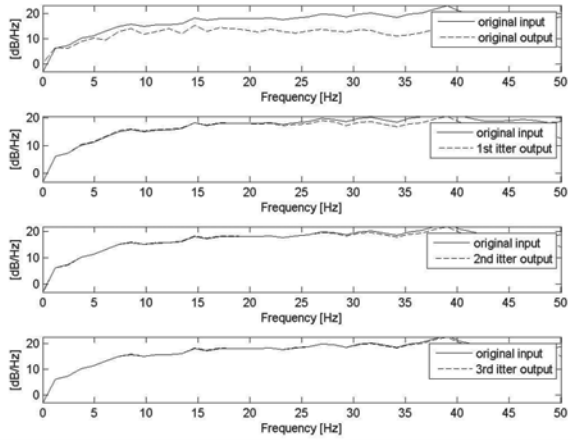

Fig. 9. PSD of pink noise for test rig (velocity)

Table 5.
Amplitude extremes for pink noise profile correction

	Original signal	
	Min [mm]	Max [mm]
Initial Input	-1.93	2.05
Initial Output	-1.63	1.65
	Test rig model	
1 iteration	-1.79	1.93
2 iteration	-1.82	1.99
3 iteration	-1.82	2.03
	Test rig	
1 iteration	-1.83	1.96
2 iteration	-1.87	1.93
3 iteration	-1.86	1.97

Table 5 presents amplitude extremes for pink noise profile correction for model and test rig respectively.

The same presentation approach has been used for white noise correction process: Fig. 10, Fig. 11, Fig. 12 for test rig model, Fig. 13, Fig. 14, Fig. 15 for physical test rig.

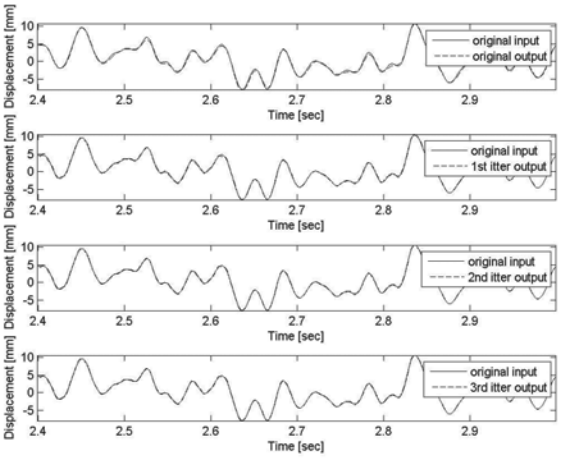

Fig. 10. White noise profile correction using test rig model

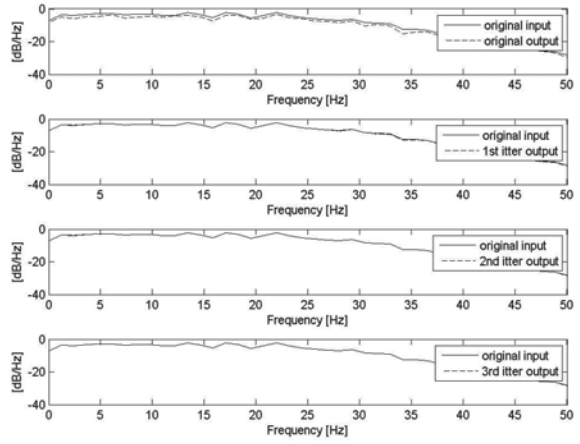

Fig. 11. PSD of white noise for test rig model (displacement)

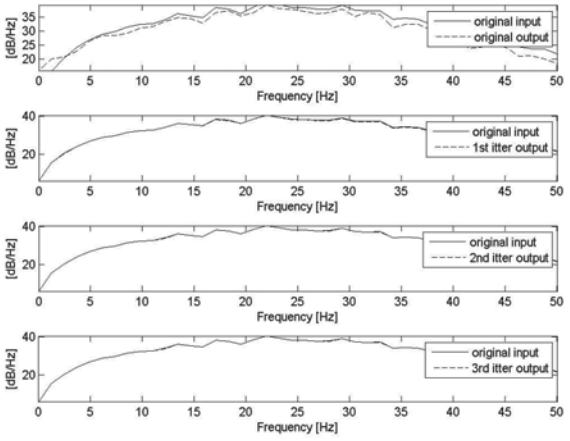

Fig. 12. PSD of white noise for test rig model (velocity)

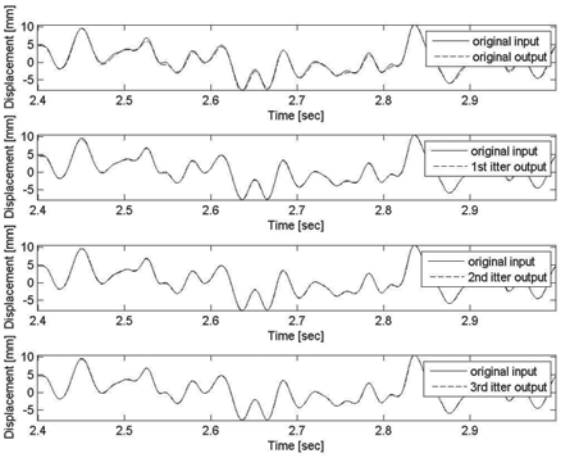

Fig. 13. White noise profile correction using test rig

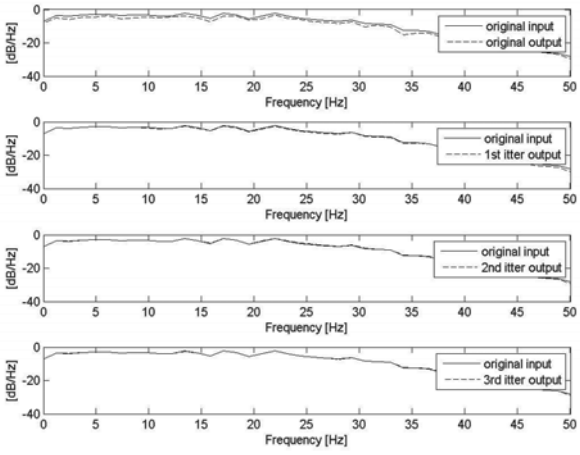

Fig. 14. PSD of white noise for test rig (displacement)

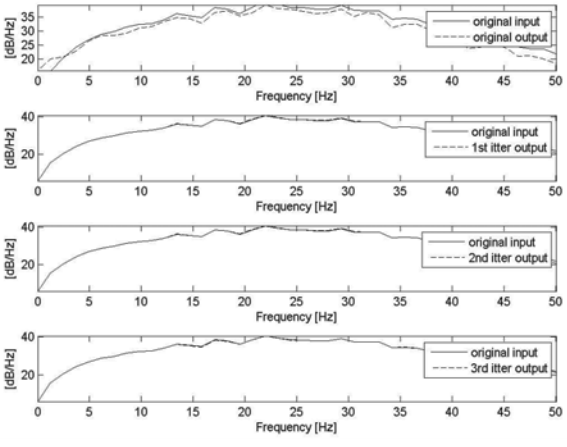

Fig. 15. PSD of white noise for test rig (velocity)

Table 6.
Amplitude extremes for white noise profile correction

	Original signal	
	Min [mm]	Max [mm]
Initial Input	-11.33	11.73
Initial Output	-11.81	12.06
Test rig model		
1 iteration	-11.33	11.73
2 iteration	-11.37	11.89
3 iteration	-11.37	11.91
Test rig		
1 iteration	-11.05	11.92
2 iteration	-11.42	11.98
3 iteration	-11.18	12.02

Table 6 presents amplitude extremes for white noise profile correction for model and test rig respectively.
Conclusions:

- Low-energetic signals need less iterations (already the first one gives the final results).
- High-energetic signals need more iterations (at least 3).
- The FFT method allows choosing the frequency band for correction process (e.g. already known hardware limitation).

5. Summary

This paper presents an approach towards improving the test rig performance for road signals used in automotive shock absorber tests. The goal is to develop a method for correction of the test signal profile in the off-line mode. The method Suitable method in case of avoidance of hardware parameters changes (e.g. PID settings). The authors performed the feasibility study applying the non-parametric approach to improve tracking of the test signal on the servo-hydraulic test rig Hydropuls® MSP25 equipped with the electronic controller IST8000 [9].

The validation of the proposed correction method was conducted using a servo-hydraulic test rig and its first-principles model. The model is capable of capturing key dynamical properties over a wide operating range while being only moderately complex. The investigations performed in the paper confirmed a strong correlation between experimental and simulation results. Therefore the model can be used for virtual evaluation of the performance of the correction method. The proposed method, both in the frequency and time domain, improves the tracking of the test signal by 10% and allows an accuracy of more than 99% and 89% to be gained using the best fit measure in the case of reproduction of white noise and pink noise signals respectively. In case of the noise signal the good results were achievable after 1-2 iterations. The pink noise signal is more difficult in reproduction since it has a flat characteristic in the frequency domain. In case of the pink signal 3 iterations were required. Nevertheless, more iterations did not improve the quality of the reconstructions. It might be caused by limited pass-band of the servo-valve which shows a drop at higher frequencies.

Off line cancellation has a limitation in case when the amplitude of the excitation cannot be modified (e.g. geometrical properties of a specimen).

More advanced model-based methods for performing off-line error correction can be considered. These methods can be used if an accuracy close to 100% is expected.

Acknowledgements

The author gratefully acknowledges the financial support of the research project N502 337636 funded by the Polish Ministry of Science (MNiI).

Nomenclature

t	continues time domain,
$x(t)$	the n-dimensional state vector,
$u(t)$	input,
$y(t)$	output,
K	bulk modulus of oil (oil stiffness) [N/m^2],
F	load [N],
x_{spool}	displacement of servo valve spool [m],
$x_{spool,min}$	lower position of servo valve spool [m],
$x_{spool,max}$	upper position of servo valve spool [m],
$x_{spool,0}$	dead zone of servo valve spool [m],
K_e	voltage-current amplifier proportional gain [A/V],
K_{spool}	current-displacement proportional gain [m/A],
K_P	PID proportional gain [V/m],
K_I	PID integral gain [V·s/m],
K_D	PID derivative gain [V/(m·s)],
K_F	feed forward proportional gain [V/m],
T_I	PID integral time [s],
T_D	PID derivative time [s],
T_f	feed forward PID derivative time [s],
x_4	displacement of actuator [m],
$x_{4,expected}$	expected displacement of actuator [m],
Δx_4	difference between expected and obtained displacement of actuator [m],
u	spool voltage [V],
u_{PID}	output voltage from PID controller [V],
u_{FF}	output voltage from feed forward gain [V],
p_A	pressure in the upper actuator chamber (chamber A) [Pa],
p_B	pressure in the lower actuator chamber (chamber B) [Pa],
p_P	pressure at the input of actuator (supply pump pressure) [Pa],
p_T	pressure at the output of actuator [Pa],
Δp_{PA}	pressure drop between input and lower chamber of actuator [Pa],
Δp_{PB}	pressure drop between input and upper chamber of actuator [Pa],
Δp_{AT}	pressure drop between lower chamber and output of actuator [Pa],
Δp_{BT}	pressure drop between upper chamber and output of actuator [Pa],
Δp_{AB}	pressure drop between lower and upper chamber of actuator [Pa],
q_A	sum of inflows and outflows to lower chamber of actuator [m^3/s],
q_B	sum of inflows and outflows to upper chamber of actuator [m^3/s],
q_{PA}	flow from input to lower chamber of actuator [m^3/s],
q_{PB}	flow from input to upper chamber of actuator [m^3/s],
q_{AT}	flow from lower chamber to output of actuator [m^3/s],
q_{BT}	flow from upper chamber to output of actuator [m^3/s],
q_{AB}	leakage flow from lower to upper chamber of actuator [m^3/s],
Cd	flow coefficient [-],
b	width of servovalve flow hole [m],
A_A	area of cross-section of lower chamber of actuator [m^2],
A_B	area of cross-section of upper chamber of actuator [m^2],
$A_{leakage}$	area of leakage between upper and lower chamber of actuator [m^2],
V_A	volume of lower chamber of actuator [m^3],
V_B	volume of upper chamber of actuator [m^3],
V_{A0}	initial volume of lower chamber of actuator [m^3],
V_{B0}	initial volume of upper chamber of actuator [m^3],
m_4	mass of moving part of actuator (actuator piston, actuator rod, adapter) [m],
c_4	fixation adapter damping coefficient [N·s/m],
c_{act}	actuator damping coefficient [N·s/m],

References

[1] J. De Cuyper, H. De Keersmaecker, J. Swevers, D. Coppens, Design of a multivariable feedback control system to drive durability test rigs in the automotive industry, Proceedings of the 5th European Control Conference, Karslruhe, Germany, 1999.

[2] J. De Cuyper, J. Swevers, M. Verhaegen, P. Sas, HN Feedback control for signal tracking on a 4 poster in the automotive industry, Proceedings of the International Seminar on Modal Analysis, Leuven, Belgium, 2000, 61-68.

[3] E. Świtoński, A. Mężyk, S. Duda, S. Kciuk, Prototype magnetorheological fluid damper for active vibration control system, Journal of Achievements in Materials and Manufacturing Engineering 21/1 (2007) 55-62.

[4] T. Dzitkowski, A. Dymarek, Design and examining sensitivity of machine driving systems with required frequency spectrum, Journal of Achievements in Materials and Manufacturing Engineering 26/1 (2008) 49-56.

[5] J. De Cuyper, D. Coppens, C. Liefooghe, J. Swevers, M. Verhaegen, Advanced drive file development methods for improved service load simulation on multi axial durability test rigs. Proceedings of the International Acoustics and Vibration Asia Cconference, Singapore, 1998, 339-354.

[6] K. Smolders, M. Volckaert, J. Swevers, Tracking control of nonlinear lumped mechanical continuous-time systems: A model-based iterative learning approach, Mechanical Systems and Signal Processing 22 (2008) 1896-1916.

[7] J. Świder, G. Wszołek, Vibration analysis software based on a matrix hybrid graph transformation into a structure of a block diagram method, Journal of Materials Processing Technology 157-158 (2004) 256-261.
[8] J. Świder, P. Michalski, G. Wszołek, Physical and geometrical data acquiring system for vibration analysis software, Journal of Materials Processing Technology 164-165 (2005) 1444-1451.
[9] Instron Structural Testing Systems – Reference Manual M32-13770-EN.
[10] G. Schothorst, Modeling of Long-Stroke Hydraulic Servo-System for Flight Simulator Motion Control and System Design, PD Thesis, Technical University of Delft, 1997.
[11] K. Białas, Reverse task of passive and active mechanical systems, Journal of Achievements in Materials and Manufacturing Engineering 23/2 (2007) 167-174.
[12] K. Białas, Synthesis of mechanical systems including passive or active elements, Journal of Achievements in Materials and Manufacturing Engineering 26/1 (2008) 67-74.
[13] MATHWORKS Inc., Matlab System Identification Toolbox Guide, Natick, MA: The Mathowrks Inc, 2007.